Available online at www.sciencedirect.com

ScienceDirect

Ceramics International 40 (2014) 2381–2388

CERAMICS INTERNATIONAL

www.elsevier.com/locate/ceramint

Fabrication and characterization of micro-dimple array on Al_2O_3 surfaces by using a micro-tooling

Taposh Roy[a], Dipankar Choudhury[a,b,*], Azuddin Bin Mamat[c], Belinda Pingguan-Murphy[a]

[a]Department of Biomedical Engineering, Faculty of Engineering, University of Malaya, 50603 Kuala Lumpur, Malaysia
[b]Faculty of Mechanical Engineering, Brno University of Technology, Technická 2896/2, 616 69 Brno, Czech Republic
[c]Department of Mechanical Engineering, Faculty of Engineering, University of Malaya, 50603 Kuala Lumpur, Malaysia

Received 9 July 2013; accepted 2 August 2013
Available online 22 August 2013

Abstract

Al_2O_3 is a material with high potential for use in biomedical implants because of its low wear rate and excellent biocompatibility. The micro-dimpling surface technique is one of the most advanced surface modification techniques available for the optimisation of tribological performance. A well-defined dimple surface fabricated on an Al_2O_3 substrate could further improve its tribological properties, thus extending the durability of an implant. In this study, we fabricated a well-defined micro-dimple pattern on an Al_2O_3 surface by using a CNC micro machine, and characterised the fabricated dimple parameters. Mechanical analyses were conducted to investigate whether there are any changes in mechanical properties, and XRD testing was performed to detect the presence of foreign wear particles due to the fabrication procedures. Finally a friction testing was conducted replicating ceramic-on-ceramic hip joints. The outcomes of the study indicate the successful fabrication of three micro-dimple patterns averaging in diameter of 403.59 μm (SD 6.6325 μm) and averaging in depth of 20.97 μm (SD 2.1368 μm). There was a change in hardness, toughness and residual strength found in subsequent mechanical testing; nevertheless, no foreign wear debris was detected. Therefore, we conclude that the precision fabrication of a micro-dimple array of Al_2O_3 surfaces by using micro-tooling can be successfully executed without any significant degradation of mechanical properties. The tribology test showed a significant reduction in friction coefficient with these micro-dimple arrays.
© 2013 Elsevier Ltd and Techna Group S.r.l. All rights reserved.

Keywords: Al_2O_3; Surface texturing; Micro-fabrication; Micro-tooling

1. Introduction

Al_2O_3 has attracted the attention of biomedical scientists, orthopedic surgeons and arthroplasty patients due to its excellent bio-tribological properties such as low wear and friction rate, high scratch resistance, and excellent biocompatibility [1]. Micro-texturing techniques, such as dimpling and honed surface techniques, are widely employed in engineering systems for good lubrication distribution, high hydrodynamic pressure and large film thickness [2–12]. Recent research shows that the scope for applying surface texturing to artificial load bearing interfaces has a high potential, particularly in storing wear debris, thus reducing the third body abrasive wear rate [13–16] and lowering the risk of an adverse biological response to micro- or nano-wear debris in the surrounding tissue. Therefore, fabrication of a dimple surface on an Al_2O_3 substrate could result in improved biotribology and durability to meet the demands of young patients.

A micro-dimple surface can be characterised by its geometric entities, such as shape (square, circular, or elliptical), equivalent diameter (20 μm–4 mm) area ratio (7–40%), and depth (200 nm–100 μm) [2,3,6,8,9,14]. All these parameters have been found to have an influence on tribological performance [10,13]. Therefore, controlling the accurate replication of dimple parameters is very important for the production of a high quality dimple surface. There are a number of machining process techniques which can be applied to fabricate micro-dimples, mostly depending on the nature of energy used for material removal. These include mechanical, thermo-electric, chemical, and electro-chemical. Mechanical and thermo-electric machining are well suited to a non-conductive material. Table 1 shows

*Corresponding author. Tel.: +60 3 79674581.
E-mail address: dipankar.choudhury78@gmail.com (D. Choudhury).

0272-8842/$ - see front matter © 2013 Elsevier Ltd and Techna Group S.r.l. All rights reserved.
http://dx.doi.org/10.1016/j.ceramint.2013.08.009

Table 1
Summary of the different types of micro-dimpling fabrication methods.

Type	Texturing process	Material	Reference
Mechanical	Abrasive jet machining	Ceramic, steel	[10]
	Shaper and sand blasting	Cast iron	[17]
	Rockwell indentation	Glass disc	[18]
Thermo-electric	Laser	Ti–6Al–4V, steel, hardened steel, Ni composite and Cr18Ni9Ti	[10,19–21]
	Electrox laser marking	Stainless steel	[2]

a few examples of micro-dimpling fabrication methods and their substrate materials as found in published literature. Laser surface texturing and photolithography micro-texturing are the most reported techniques.

Thermo-electric machining processes such as electro-discharge machining (EDM), electron beam machining (EBM), laser beam machining (LBM), and plasma-arc machining (PAM) are found to be accurate; however, their initial setup, as well as, their fabrication cost, is very high. The thermo-electric machining process may also change the bulk material properties since it produces a high temperature. Mechanical machining processes do not have these limitations; nevertheless, their accuracy for micro-fabrication in ceramics is uncertain. Micro-mechanical machining, supported by CNC (CNC micro machine), is a highly precise machining process ($\pm 1\%$ micron error) along the X, Y and Z axes. It is cost effective and applicable to non-conductive materials. However, a few researchers have raised the possibility of wear debris being trapped in the dimple from the drill bit [22,23]. This wear debris might not be biocompatible, therefore introducing risk to the implanted prosthesis. Moreover, finding a hard drill bit (harder than ceramic) with the required specification is also a key concern. So far, the application of the CNC micro machine is still limited to soft materials due to the limitations of the drill bit. In this study, we fabricated a well-defined micro-dimple surface on conventional ceramic surfaces (Al_2O_3), characterised the dimple surface in terms of its geometry and accuracy, investigated whether there is any effect on mechanical properties of the substrate surface due to the drilling process, and inspected the presence of foreign wear debris in the dimple area generated by the tool bits or surface finishing accessories. A preliminary frictional test was also conducted in order to justify its potential application to ceramic-on-ceramic hip joints.

2. Materials and methods

2.1. Sample preparation

A commercially available alumina plate (99.6% Al_2O_3, purchased from AdValue Technology Tucson, USA) at a size of $90 \times 65 \times 6\ mm^3$ was used in this study for fabrication of the micro-dimple. The Al_2O_3 plate was cut into smaller pieces ($15 \times 15 \times 6\ mm^3$) by a diamond cutter (IsoMet® 5000 Precisions Saws Buehler, China). Each sample went through a series of polishing processes in order to achieve a mirror finish. A diamond grinding disc (30 μm) was used for initial

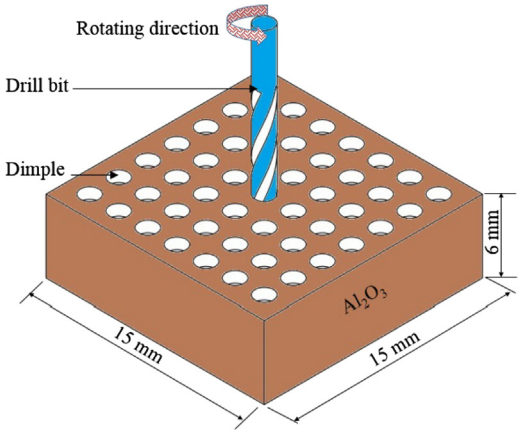

Fig. 1. Schematic of fabrication of micro-dimple by CNC micro-machine on an Al_2O_3 sample.

polishing, followed by sequential polishing with 9 μm, 6 μm, 1 μm and 0.05 μm diamond polycrystalline suspensions (DPS). A CNC micro machine (Mikrotools DT110, Singapore) was used to fabricate the micro-dimples on the Al_2O_3 sample (Fig. 1). A solid carbide drill bit (M.A Ford, USA) with diameter of 400 μm was used to create the dimples. In order to achieve effective machining, spindle speed and feed rate were maintained at 55,000 rpm and 334 mm/min respectively as per supplier recommendation. A new drill bit was used in each sample as there was a visible sign of wear on the drill bit's tip.

The key parameters for this experiment are the dimple array patterns and dimple profile, because it was previously reported that these parameters affect the tribology of a system [2,3,5,14]. 3 types of dimple array patterns with diameter and depth of each dimple being 400 μm and 20 μm, respectively, were chosen for this study (Table 2).

3. Experimental procedures

3.1. Characterisation

3.1.1. Surface roughness

The sample surface roughness, Ra, was measured using a surface profilometer (Mitutoyo sj210, USA), at random locations across the surface (5 times parallel, and 5 times transverse along 4.5 mm spans).

3.1.2. Dimple profile

The dimple array patterns were specified using CATIA software (Fig. 2). A CNC machine was used to manufacture

the dimples. Scanning electron microscopy (SEM; AURIGA, Zeiss Singapore) was used to confirm the morphology of the dimple array patterns (Fig. 3a). The diameter and the pitch (distance between 2 dimples) were measured with an optical microscope (Olympus BX51, Japan). Analysis software by Olympus, Japan, was used to measure the diameter and pitch of the dimple. Basically, a region of interest (ROI) was selected, and the software calculated the diameter. A digital ruler within the software was used to measure the distance. The depth of the dimple was measured by a surface profilometer (Mitutoyo sj210, USA). This is a stylus type of profilometer, and being tapped across the surface of the dimple, it produces a measurement along the X and Y axes. The reading from the Y axis will be used to calculate the height of the dimple (Fig. 3b). The X reading can be used to confirm the diameter of the dimple which was measured previously by an optical microscope. Each sample has 2 replicates.

Friedrich [23] mentioned the possible surface integrity caused by the cutting process, and unexpected wear debris (chips) generated which may not be completely removed from the dimple. Therefore, samples were washed with 10% sulphuric acid, distilled water and ultrasonic cleaner, and then tested with X-ray diffraction (XRD; Philips X′pert MPD PW3040, Singapore) and EDS (SEM; Philips XL40). The XRD pattern of the sample was then compared to that of Al_2O_3 (JCPDS card 46-0306). EDS was then employed to determine the presence of any other foreign particles.

3.2. Mechanical properties

3.2.1. Hardness

Vickers indentation (Mitutoyo AVK-C2, USA) technique was used to measure hardness, fracture toughness and residual stress. A 2 kg load was loaded on to the dimple and non-dimple surface area for 15 s. The length of the diagonal and crack produced by indenter is shown in Fig. 4. Three random dimples and non-dimple areas were selected for the hardness test. These procedures were repeated on every sample.

Table 2
Dimple parameters.

Dimple array pattern	Dimple diameter (μm)	Dimple distance/ pitch (mm)	Dimple depth (μm)	Dimple area density (%)
Pattern 1	400	2	20	5.84
Pattern 2	400	1.5	20	9.78
Pattern 3	400	1	20	19.63

3.2.2. Fracture toughness (K_{IC})

The fracture toughness (K_{IC}) was calculated from the length of cracks (Fig. 4) induced by the indenter using the equation [24,25]

$$K_{IC} = 0.016\left(\frac{E}{H}\right)^{1/2}\left(\frac{P}{C^{3/2}}\right) \quad (1)$$

where K_{IC} is the indentation fracture toughness (Pa $\sqrt{m}$), 0.016 is the material-independent constant for a Vickers radial crack, E is Young's modulus (MPa), H is the Vickers hardness (GPa), P is the indentation load (N), and C is the half-length of the radial cracks parallel to the layers on the surface (m). The value of $0.016\left(\frac{E}{H}\right)^{1/2}$ was estimated at 0.07, which is a typical value for Al_2O_3 ceramics.

3.2.3. Residual stress

Residual stresses within the dimple surface were also calculated by indentation methods. In low surface tension conditions, cracks perpendicular to the layers (C_R) were determined by the stress intensity factor for the crack under stress. The indentation fracture toughness (K_{IC}) was related to two factors; the first was the stress intensity factor for the crack under stress (K_I), which caused deformation of the area by indentation, and the second was residual stress represented by K_R:

$$K_{IC} = K_I + K_R \quad (2)$$

$$K_R = Y\sigma_R C_R^{1/2} \quad (3)$$

where Y is a geometric factor, approximately 1.26, σ_R is the residual stress, and (C_R) is the crack perpendicular to the layer. The residual stress on both sides of the crack was the same, whereas this was not the case in the field gradient. The values recorded indicated that the residual stresses were at the centre of the indentation. The stress was tensile when $\sigma_R > 0$ and compressive when $\sigma_R < 0$:

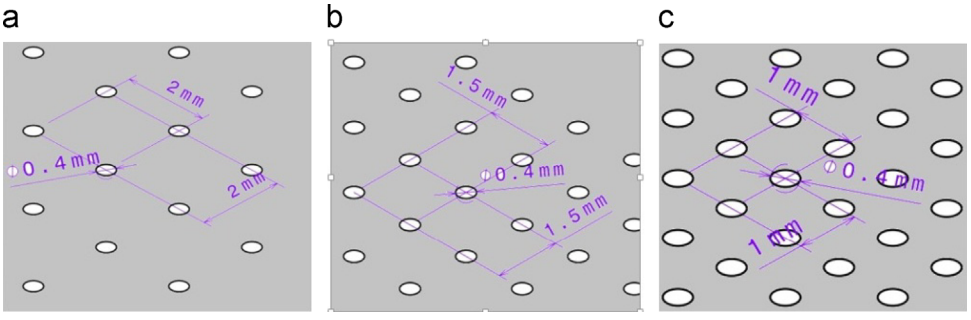

Fig. 2. A drawing of the 3 dimple array patterns. The dimple array pattern is arranged in a rectangular pattern. (a) In pattern 1, the distance between 2 dimples is 2 mm, (b) in pattern 2, the distance between 2 dimples is 1.5 mm, and (c) in pattern 3, the distance between 2 dimples is 1 mm.

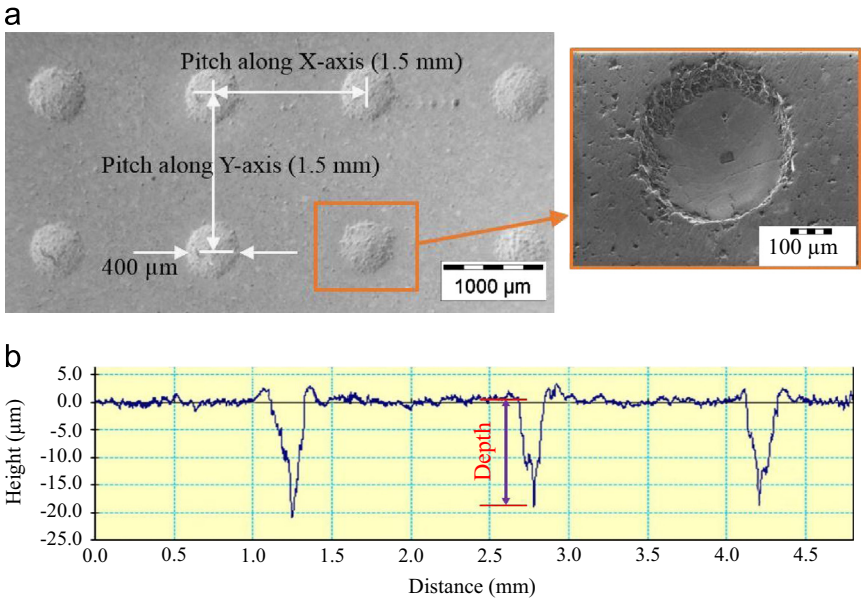

Fig. 3. (a) A SEM image shows the micrograph of pattern 2 surface, and (b) dimple profiles were mapped by the profilometer where their depths are shown by the red arrow. (For interpretation of the references to colour in this figure legend, the reader is referred to the web version of this article.)

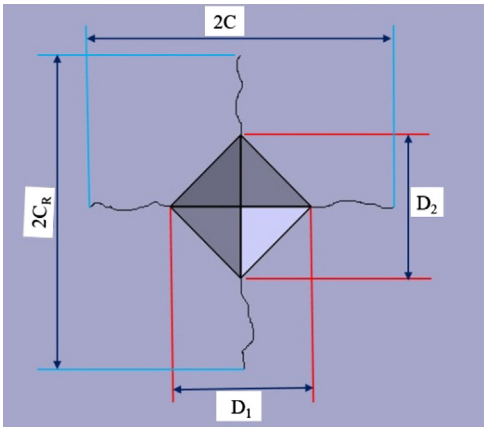

Fig. 4. Crack indentation definition by Vickers indenter.

$$\sigma_R = \frac{K_{IC} - K_I}{Y C_R^{1/2}} = \frac{K_{IC}\left[1 - \left(\frac{C}{C_R}\right)^{3/2}\right]}{Y C_R^{1/2}} \quad (4)$$

The main difficulty involved in measuring hardness within the dimple is dealing with the curved surface. Since the 3D topography for a dimple is similar to a semispheroid, measurement error is unavoidable. To minimise the experimental error the Vickers indenter was chosen as it has a better stability when dealing with curved surfaces than do other common indenter types.

3.3. Friction testing

Friction tests were conducted by a pin-on-disk tester (Fig. 5) where the disk (flat surface) and pin (cylindrical surface) were rubbing each other. The disks had three surface profiles: non-dimple, pattern 1 and pattern 2 which were investigated under bovine calf serum. The pin was placed into a metallic holder (zero degree of freedom), and the holder had 10 mm/s speed (simulated medium walking speed 10 mm/s) and was loaded under 10 N, 15 N, 20 N. Details of experiment parameters are shown in Table 3. The sliding contact zone was fully soaked in a lubricant where the temperature was kept at 37 °C throughout the tests.

Friction coefficients were calculated using the friction force measured at different loading conditions. Total running time of every sample was 90 min—first 30 min under 10 N, next 30 min under 15 N, and last 30 min under 20 N. These loads were estimated to create the Hertzian contact pressure of 0.132, 0.162, and 0.187 GPa correspondingly.

4. Result and discussion

4.1. Surface roughness

Prior to the fabrication of the dimples, the sample Ra was measured. The average surface roughness (Ra) of six samples was 0.12 ± 0.02 µm, indicating that the prepared samples have a smooth surface. The very small standard error measurement of the 6 samples shows that almost all the samples have the same surface roughness.

4.2. Dimple profile

The morphologies of the dimple array patterns were confirmed by SEM images (Fig. 6). Table 4 summarises the measured and theoretical values of the dimple diameter, depth and pitch along X and Y. It shows that measured and theoretical values are very close and the standard deviation is very small in all cases. This confirms that the CNC micro machine can be used to produce micro-dimples with accuracy. The tribology of a system depends on the diameter, depth and

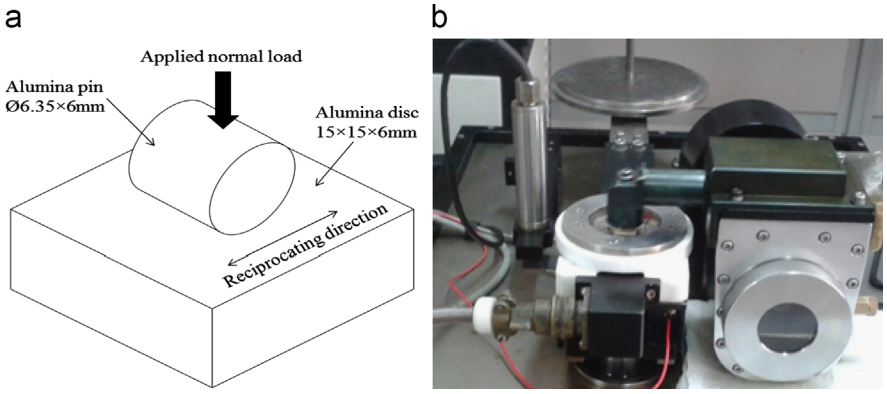

Fig. 5. (a) Schematic diagram of the test setup and (b) tribometer.

Table 3
Parameters of friction test.

Pin and disc	Alumina ceramic
Load (N)	10, 15, 20
Hertz contact pressure (GPa)	0.132, 0.162, 0.187
Sliding velocity (mm/s)	10
Stroke length (mm)	2
Lubricant	Bovine synovial fluid
Temperature (°C)	37

pitch distance [14,19,22]; hence we needed to make sure the selected parameters are reproducible. The ability of the CNC micro machine to control accurate replication of dimple parameters allows the production of a high quality dimple surface.

4.3. Debris

The results of the wear debris (chips) tests were likewise supportive of the manufacture method. The XRD pattern from the cleaned sample is shown in Fig. 7, which coincides with that of aluminium oxide in the JCPDS card of 46-0306. Based on the XRD result, there is no other foreign particle found on the surface of the sample. The EDS pattern also showed no other foreign particle inside the dimple in Fig. 8.

4.4. Mechanical properties

Mechanical testing including hardness, toughness and residual test was performed in view of the brittleness properties of the ceramic. A pile-up region was observed on the outer edge of the dimple, a phenomenon often associated with tensile stress and a negative influence on tribological properties. As a result of the pile-up regions, compressive residual stresses are formed on the material subsurface. Micro-machining does not affect the hardness within the dimple area. The average hardness within the dimple area was slightly lower than the average value of the non-dimple area. This could be explained by the presence of compressive stress within the dimple surface. On average, hardness in the dimple area decreased 13% compared to the bulk material. Fig. 9 presents the hardness profile of the surface for different patterns. As the dimple depth is 20 μm, the slope of the dimple is nearly perpendicular to the surface.

The fracture toughness of the dimple surfaces at the applied indentation load of 2 kg is shown in Fig. 10. At the centre of the dimple the fracture toughness was as low as 3.9 MPa $\sqrt{m}$ increasing at the periphery of the dimple, where fracture toughness on the non-dimple surface averaged to 6.5 MPa $\sqrt{m}$. As compressive load was applied during the drilling process at the centre of the dimple, fracture toughness is less there than in the non-dimple surface areas. Fig. 11 shows that compressive residual stress forms at the centre of the dimple, but near the periphery of the dimple diameter there is tensile residual stress due to the pile-up region, as expected. It is expected that tensile residual stress creates the premises for crack initiation and crack growth. On the other hand, compressive residual stresses on the surface act on surface integrity by closing crack tips and resisting crack growth [26]. At the dimple centre the residual stresses were measured at 385, 381 and 376 MPa (compressive) whereas near the pile-up region the residual stresses were measured at 150, 201 and 173 MPa (tensile).

4.5. Friction test

The friction coefficient profiles for non-dimple, and patterns 1 and 2 are shown in the Fig. 12. The average friction coefficient (μ) trends were found to be as follows:

$\mu_{\text{pattern 2}} < \mu_{\text{pattern 1}} < \mu_{\text{non-dimple}}$At load 10 N (132 Mpa), the performance of dimple surface was very significant—the percentage of friction coefficient reduction 15.2% to pattern 2 and 9.1% to pattern 1 compared to non-dimple surface. However, the difference of friction coefficient became flatter at the higher load 20 N (187 Mpa)—percentage of friction coefficient reduction 3.6% to the pattern 2 and 3.2% to pattern 1 compared to non-dimple surface. Although both dimple surfaces (Patterns 1 and 2) showed good friction reduction, it also revealed that the micro-dents with higher area density performed better in reducing friction. This might be because the higher density dimple area had better fluid reservation and promoted the retention of a thicker lubricating film.

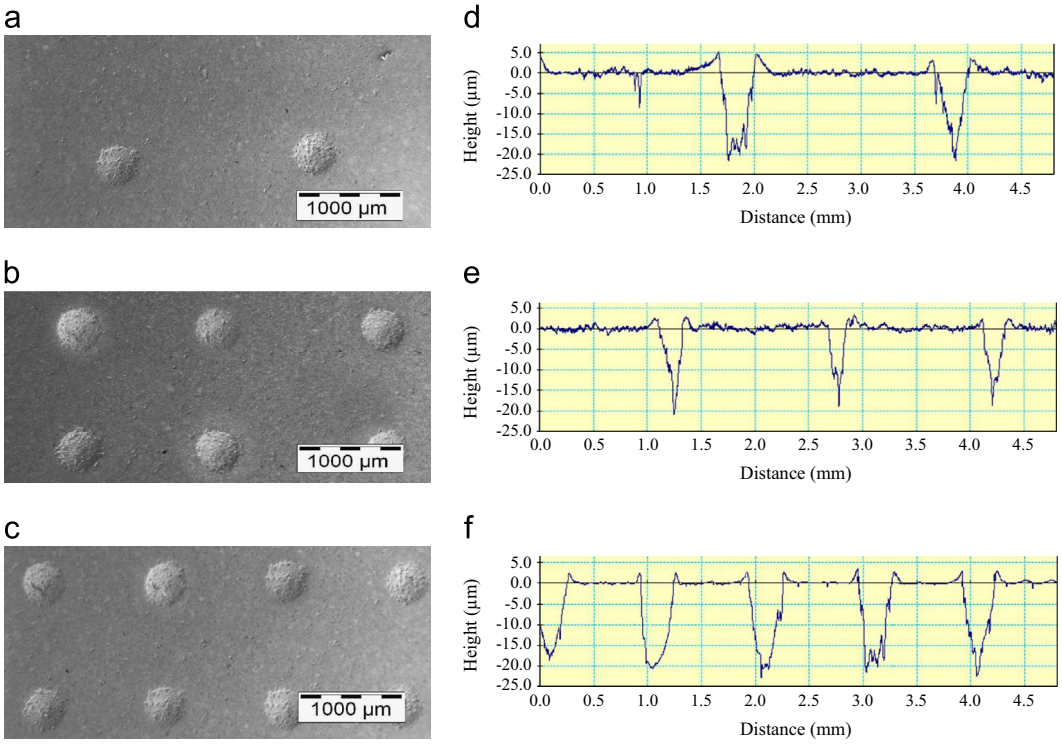

Fig. 6. (a)–(c) Morphologies of the 3 dimple array patterns imaged by SEM, and (d)–(f) profiles of the 3 dimple array patterns mapped by the profilometer.

Table 4
Comparison of dimple parameters of theoretical and measured values.

Dimple parameters		Pattern 1 (total 98 dimples)		Pattern 2 (total 162 dimples)		Pattern 3 (total 338 dimples)	
		Theoretical value	Measured value	Theoretical value	Measured value	Theoretical value	Measured value
Diameter (μm)	Mean	400.00	404.84	400.00	403.59	400.0	404.58
	SD	–	5.55	–	6.63	–	5.37
Depth (μm)	Mean	20.00	21.34	20.00	20.97	20.0	21.62
	SD	–	2.17	–	2.14	–	2.60
Pitch along *X*-axis (mm)	Mean	2.00	1.98	1.50	1.50	1.00	0.95
	SD	–	0.03	–	0.03	–	0.02
Pitch along *Y*-axis (mm)	Mean	2.00	1.97	1.50	1.49	1.00	0.94
	SD	–	0.01	–	0.02	–	0.01

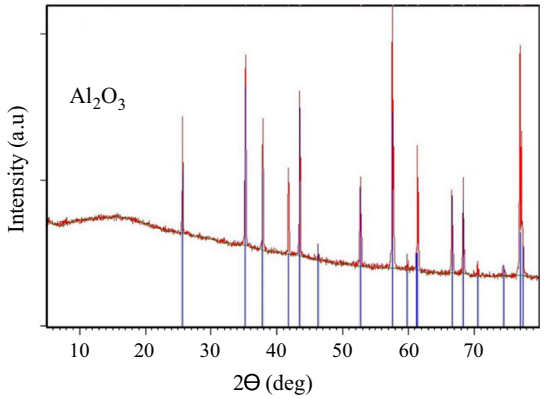

Fig. 7. XRD pattern of the dimple surface.

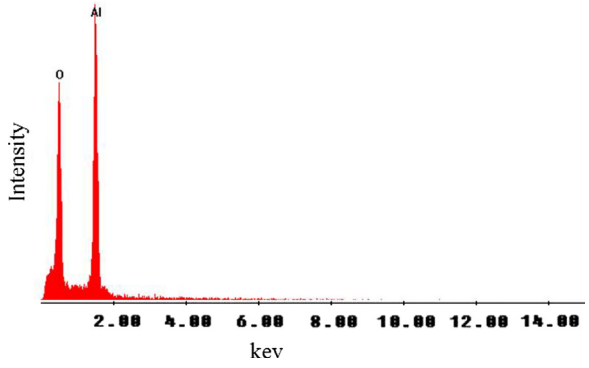

Fig. 8. EDS pattern of the selected area inside the dimple surface.

In addition, an increase of the dimple density alone resulted in a decrease of the direct contact area. Again, at higher load, perhaps, the produced film could not withstand the applied load. However, a film thickness measurement could justify this mechanism better. Unfortunately, the tribology simulator was not capable of measuring that tribological parameter. Moreover, we did not consider wear rate measured by the tribology

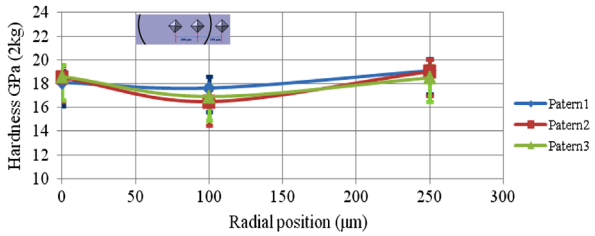

Fig. 9. Vickers hardness for the dimple surface with load 2 kg.

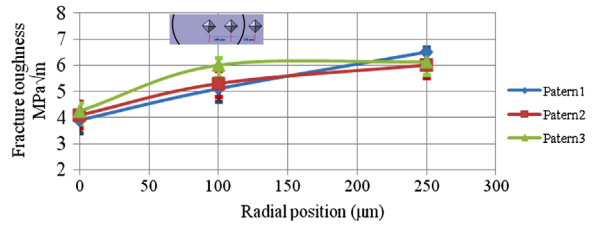

Fig. 10. Indentation fracture toughness for the dimple surface.

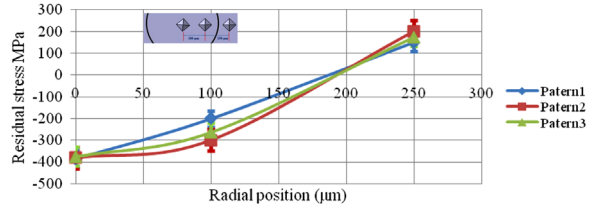

Fig. 11. Residual stress measured by the indentation method for the dimpling surface.

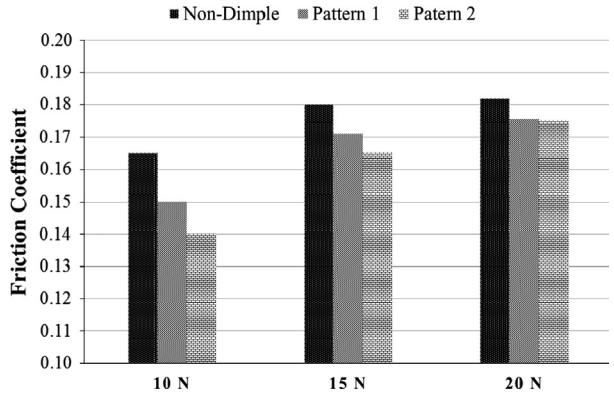

Fig. 12. Friction coefficients for different samples at 10 N, 15 N, and 20 N loads.

simulator since it was affected by the wear debris. However the reduction of friction coefficient is justified by other similar published studies, although they were conducted on other material combinations [13,27,28].

Despite these limitations, realistic simulated hip joints experiment conditions were maintained. These parameters are: (1) bovine synovial fluid, which was collected from four joints of a cow [29]; (2) loads of 10, 15, 20 N (Hertz pressure 132, 162, 187 MPa) which are similar to those of other published articles for ceramic-on-ceramic hip joints [30]; (3) speed of 10 mm/s which is simulated medium walking speed [31]; (4) 37 °C temperature which is body temperature [29]; and (5) a very smooth surface (Ra 0.12 μm) [13].

5. Conclusion

A successful fabrication of micro-dimple array on Al_2O_3 surfaces revealed the feasibility of applying micro-tools on ceramic surfaces. The key findings of this research are as follows:

i. Micro-tooling is a reliable process for fabricating micro-dimple arrays with different geometries on ceramic surfaces. The dimple parameters were precisely characterised (diameter, depth, pitch along *X*-axis, pitch along *Y*-axis), each with standard deviation as low as 3.75%.
ii. The hardness was found to be 9.8% and 2.5% lower at the inner edge and centre of the dimple respectively, compared to the non-dimple area. Moreover, the centre of the dimple was found to have a lower toughness compared to the inner edge and non-dimple area. The induced residual stress was compressive (380.67 MPa) at the centre of the dimple.
iii. There was no detectable wear debris nor were there cutting chips found in the dimple holes.
iv. Friction test confirmed the influence of dimple surface in significantly reducing friction coefficient at 10–20 N loads under simulated hip joint conditions. A further tribological experiment with wide ranges of dimple parameters on optimising dent surfaces to ceramic on ceramic hip joints based on their outcomes on friction, wear rate and load carrying capacity is under investigation.

Acknowledgements

The research was supported by University of Malaya Research Grant (UMRG; RG147-12AET) and Ministry of Higher Education High ImpactResearch Grant (UM.C/HIR/MOHE/ENG/44).

References

[1] H.S.A. Rahman, D. Choudhury, N.A.A. Osman, H.N. Shasmin, W.A.B.W. Abas, In vivo and in vitro outcomes of alumina, zirconia and their composited ceramic-on-ceramic hip joints, Journal of the Ceramic Society of Japan 121 (4) (2013) 382–387.
[2] Y. Qiu, M. Khonsari, Experimental investigation of tribological performance of laser textured stainless steel rings, Tribology International 44 (5) (2011) 635–644.
[3] S. Qian, D. Zhu, N. Qu, H. Li, D. Yan, Generating micro-dimples array on the hard chrome-coated surface by modified through mask electrochemical micromachining, The International Journal of Advanced Manufacturing Technology 47 (9–12) (2010) 1121–1127.
[4] W. Huang, L. Jiang, C. Zhou, X. Wang, The lubricant retaining effect of micro-dimples on the sliding surface of PDMS, Tribology International (2012).

[5] A. Kovalchenko, O. Ajayi, A. Erdemir, G. Fenske, I. Etsion, The effect of laser surface texturing on transitions in lubrication regimes during unidirectional sliding contact, Tribology International 38 (3) (2005) 219–225.
[6] F. Meng, T. Davis, J. Cao, Q.J. Wang, D. Hua, J. Liu, Study on effect of dimples on friction of parallel surfaces under different sliding conditions, Applied Surface Science 256 (9) (2010) 2863–2875.
[7] X. Wang, K. Kato, K. Adachi, K. Aizawa, Loads carrying capacity map for the surface texture design of SiC thrust bearing sliding in water, Tribology International 36 (3) (2003) 189–197.
[8] M.-s. Suh, Y.-h. Chae, S.-s. Kim, T. Hinoki, A. Kohyama, Effect of geometrical parameters in micro-grooved crosshatch pattern under lubricated sliding friction, Tribology International 43 (8) (2010) 1508–1517.
[9] X. Wang, W. Liu, F. Zhou, D. Zhu, Preliminary investigation of the effect of dimple size on friction in line contacts, Tribology International 42 (7) (2009) 1118–1123.
[10] M. Wakuda, Y. Yamauchi, S. Kanzaki, Y. Yasuda, Effect of surface texturing on friction reduction between ceramic and steel materials under lubricated sliding contact, Wear 254 (3) (2003) 356–363.
[11] D. Choudhury, R. Walker, A. Shirvani, R. Mootanah, The influences of honed surfaces on metal-on-metal hip joints, Tribology Online 8 (3) (2013) 195–202.
[12] D. Choudhury, R. Walker, T. Roy, S. Paul, R. Mootanah, Performance of honed surface profiles to artificial hip joints: an experimental investigation, International Journal Of Precision Engineering And Manufacturing (2013) (in press).
[13] H. Sawano, S.i. Warisawa, S. Ishihara, Study on long life of artificial joints by investigating optimal sliding surface geometry for improvement in wear resistance, Precision Engineering 33 (4) (2009) 492–498.
[14] L. Gao, P. Yang, I. Dymond, J. Fisher, Z. Jin, Effect of surface texturing on the elastohydrodynamic lubrication analysis of metal-on-metal hip implants, Tribology International 43 (10) (2010) 1851–1860.
[15] P. Shum, Z. Zhou, K. Li, To increase the hydrophobicity and wear resistance of diamond-like carbon coatings by surface texturing using laser ablation process, Thin Solid Films (2013) (in press).
[16] X.J. Jiang, D.J. Whitehouse, Technological shifts in surface metrology, CIRP Annals—Manufacturing Technology 61 (2) (2012) 815–836.
[17] M. Nakano, A. Korenaga, A. Korenaga, K. Miyake, T. Murakami, Y. Ando, H. Usami, S. Sasaki, Applying micro-texture to cast iron surfaces to reduce the friction coefficient under lubricated conditions, Tribology Letters 28 (2) (2007) 131–137.
[18] I. Křupka, M. Hartl, The effect of surface texturing on thin EHD lubrication films, Tribology International 40 (7) (2007) 1100–1110.
[19] T. Hu, L. Hu and Q. Ding, Effective solution for the tribological problems of Ti–6Al–4V: combination of laser surface texturing and solid lubricant film, Surface and Coatings Technology 206 (24) (2012), 5060–5066.
[20] A. Kovalchenko, O. Ajayi, A. Erdemir, G. Fenske, Friction and wear behavior of laser textured surface under lubricated initial point contact, Wear 271 (9) (2011) 1719–1725.
[21] J. Li, D. Xiong, H. Wu, Y. Zhang and Y. Qin, Tribological properties of laser surface texturing and molybdenizing duplex-treated stainless steel at elevated temperatures, Surface and Coatings Technology 228, Supplement 1, (2012), S219–S223.
[22] Y. Guo, R. Caslaru, Fabrication and characterization of micro dent arrays produced by laser shock peening on titanium Ti–6Al–4V surfaces, Journal of Materials Processing Technology 211 (4) (2011) 729–736.
[23] C. Friedrich, Micromechanical machining of high aspect ratio prototypes, Microsystem Technologies 8 (4–5) (2002) 343–347.
[24] S. Gustafsson, L.K.L. Falk, E. Lidén, E. Carlström, Pressureless sintered Al_2O_3–SiC nanocomposites, Ceramics International 34 (7) (2008) 1609–1615.
[25] E. Askari, M. Mehrali, I. Metselaar, N. Kadri, M.M. Rahman, Fabrication and mechanical properties of functionally graded material by electrophoretic deposition, Journal of the Mechanical Behavior of Biomedical Materials (2012).
[26] Y.B. Guo, R. Caslaru, Fabrication and characterization of micro-dent arrays produced by laser shock peening on titanium Ti–6Al–4V surfaces, Journal of Materials Processing Technology 211 (4) (2011) 729–736.
[27] H. Ito, K. Kaneda, T. Yuhta, I. Nishimura, K. Yasuda, T. Matsuno, Reduction of polyethylene wear by concave dimples on the frictional surface in artificial hip joints, The Journal of Arthroplasty 15 (3) (2000) 332–338.
[28] C. Myant, R. Underwood, J. Fan, P. Cann, Lubrication of metal-on-metal hip joints: the effect of protein content and load on film formation and wear, Journal of the Mechanical Behavior of Biomedical Materials 6 (2012) 30–40.
[29] V.C. Mow, R. Huiskers, Basic Orthopaedic Biomechanics and Mechano-Biology, Lippincott Williams & Wilkins, 2005.
[30] L. Mattei, F. Di Puccio, B. Piccigallo, E. Ciulli, Lubrication and wear modelling of artificial hip joints: a review, Tribology International 44 (5) (2011) 532–549.
[31] G. Bergmann, G. Deuretzbacher, M. Heller, F. Graichen, A. Rohlmann, J. Strauss, G. Duda, Hip contact forces and gait patterns from routine activities, Journal of Biomechanics 34 (7) (2001) 859–871.